Nuclear Instruments and Methods in Physics Research A 1089 (2026) 171542

Contents lists available at ScienceDirect

Nuclear Inst. and Methods in Physics Research, A

journal homepage: www.elsevier.com/locate/nima

Full Length Article

Design, assembly and beam validation of a full-scale TORCH module ☆

A. Abdelmotteleb [i], M. Adinolfi [a], M. Armour [i], T. Blake [i], T. Conneely [h], D. Cussans [a], A. Davidson [i], S. Dekkers [f], R. Dzhygadlo [j], U. Egede [f], T.C. Fearon [a], C. Frei [b], R. Forty [b], R. Gao [g], T. Gershon [i], T. Gys [b], T. Hadavizadeh [f], G. Hallett [i], N. Harnew [g], D. Hu [k], K. Jewkes [i], M. Kreps [i], J. Lapington [e], M. Lehuraux [i,*], P. Li [c], J. Liu [k], A. Lowe [g], M. Loutit [a], T. Ma [k], I. Mackay [g], S. Malde [g], S. Mao [c], A. Markfort [h], J. Milnes [h], A. Mitra [i], R. Pestotnik [d], D. Piedigrossi [b], I. Polyakov [b], W. Qian [c], R. Rabadan [a], J. Rademacker [a], G. Schepers [j], J. Schwiening [j], M. Shao [k], T. Slater [g], S. Stanislaus [g], E. Walton [f], N. Wang [c], Y. Wang [k], B. Westhenry [a], G. Wilkinson [g], A. York [g], L. Zhu [c]

[a] University of Bristol, HH. Wills Physics Laboratory, BS8 1TL, Bristol, UK
[b] CERN, CH-1211, Meyrin, Switzerland
[c] University of Chinese Academy of Sciences, School of Physical Sciences, 100049, Beijing, China
[d] Jozef Stefan Institute, Experimental Particle Physics Department, SI-1000, Ljubljana, Slovenia
[e] University of Leicester, School of Physics and Astronomy, LE1 7RH, Leicester, UK
[f] Monash University, School of Physics and Astronomy, VIC 3800, Clayton, Australia
[g] University of Oxford, Denys Wilkinson Building, OX1 3RH, Oxford, UK
[h] Photek Ltd, 26 Castleham Rd, TN38 9NS, Saint Leonards-on-sea, UK
[i] University of Warwick, Department of Physics, CV4 7AL, Coventry, UK
[j] GSI Helmholtzzentrum für Schwerionenforschung GmbH, Planckstraße 1, 64291, Darmstadt, Germany
[k] University of Science and Technology of China, School of Physics, 230026, Hefei, China

ARTICLE INFO

Keywords:
Particle identification
Time-of-flight

ABSTRACT

The TORCH time-of-flight detector is part of a proposed upgrade of the LHCb experiment, foreseen for the high-luminosity phase of the LHC. The TORCH detector provides particle identification of hadrons in the sub-10 GeV/c momentum range, exploiting the prompt production of Cherenkov photons in an array of fused-silica plates. Photons are propagated to the periphery of the detector via total internal reflection, where they are focused by a cylindrical mirror onto an array of fast-timing MCP-PMT photon detectors. In order to achieve the design goals of TORCH, individual photons must be timed to 70 ps precision or better. The development of the MCP-PMTs, the mechanical design and assembly strategy of a full-scale TORCH detector module, plus its system-level validation in a test beam are described. A validation of timing references, the optical integrity across glue joints and the readout integration are presented.

1. Introduction

The TORCH detector is a proposed time-of-flight system for the Upgrade II of the LHCb experiment [1], aimed at providing charged-hadron particle identification in the momentum range 2–10 GeV/c, where the separation power of the existing Ring-Imaging Cherenkov detectors for kaons and protons has to rely on the pion veto mode. The TORCH concept exploits the prompt emission of Cherenkov photons in thin fused-silica radiators, with the photon propagation and timing used to extend LHCb particle identification capabilities during the high-luminosity phase of the LHC. A detailed description of the detector principle can be found in Ref. [2].

The baseline TORCH design foresees a large-area detector composed of twelve identical modules, arranged vertically to cover a significant fraction of the LHCb acceptance. The detector would be located approximately 9.5 m from the interaction point. Each module comprises a $250 \times 66 \times 1$ cm^3 fused-silica radiator, manufactured in three sections and optically bonded to a focusing block, together with multi-anode photomultiplier (MCP-PMT) photon detectors and readout electronics.

☆ This article is part of a Special issue entitled: 'RICH2025' published in Nuclear Inst. and Methods in Physics Research, A.

* Corresponding author.
E-mail address: marion.lehuraux@cern.ch (M. Lehuraux).

https://doi.org/10.1016/j.nima.2026.171542
Received 4 February 2026; Received in revised form 20 March 2026; Accepted 29 March 2026
Available online 1 April 2026

Cherenkov photons produced when a charged particle goes through the radiator are propagated to the array of fast-timing photon detectors via total internal reflection. To minimise the material budget within the LHCb detector acceptance, the modules are supported by a rail-based mechanical structure that allows individual units to be slid into position, while concentrating the majority of services, readout and support material at the periphery of the detector.

Simulation studies and small-scale prototypes have previously demonstrated the feasibility of the TORCH concept and its expected performance [3]. Building upon this work, the present paper reports on the MCP-PMT development, the design, assembly and system-level validation of the first full-scale TORCH module, corresponding in size and geometry to a unit suitable for integration into LHCb. This first full-scale module will bring valuable insight for the work still ongoing towards the final integration design. The mechanical realisation, optical assembly strategy and integration of the complete detector chain are described. A beam test performed at the CERN PS in 2025 is used to validate the operation and stability of the assembled module in a charged particle beam.

2. Photodetector development

The TORCH detector has a requirement of 70 ps time resolution per photon in order to reach a precision of 15 ps per particle. The high-luminosity conditions of the HL-LHC correspond to a pile-up of approximately 40 interactions per bunch crossing, resulting in a high track density in the LHCb detector and, consequently, a high occupancy of the TORCH photon detectors. However to ensure good operation, the photon detector occupancy must ideally be kept below 20%. This occupancy requirement implies a need for high-granularity photon detectors, in particular in the centre-most modules closest to the LHC beam line. The detector must also withstand a neutron-equivalent fluence of up to 2×10^{12} cm^{-2} and operate at high rate, 5–25 μA cm^{-2}, depending on the module. The main photodetector candidates are MCP-PMTs and silicon photomultipliers (SiPMs). However the former are limited by their rate capabilities and lifetime, while the later have large dark count rates requiring the adoption of complex liquid-nitrogen cooling systems to reduce background rates to a manageable level. In this work, only MCP-PMTs will be discussed but R&D on SiPMs is ongoing.

The TORCH collaboration has worked with Photek-UK to develop a multi-channel square MCP-PMT with ALD-coated pores, resistive anode coupling, and with a customised TORCH granularity of 8 × 64 pixels over a 53 × 53 mm^2 square area, corresponding to 6.625×0.828 mm^2 pixels. The pixels are read out individually. The so-called TORCH Phase 3 Photek MCP-PMTs [3], first used in 2018, were utilised by TORCH in the beam tests presented in Section 4. These devices have more recently been tested in the laboratory at Photek where the rate capability of the tube as a function of gain has been measured. By optimising the resistivity of the plates used in the MCP-PMT, Photek have been able to demonstrate significant improvements in rate-capability over the original TORCH prototypes [4]. A known area of the cathode's surface was uniformly illuminated, with the remaining MCP-PMT active area masked. The laser rate was varied and the anode current measured. Results show that further improvements by at least a factor of 5 in the gain retention at high rates, at a nominal gain of 10^6, will be necessary to fulfil the TORCH requirements at the HL-LHC.

A recent TORCH and Photek collaboration is the development of a 16 × 96 MCP-PMT over a 53 × 53 mm^2 square area. This MCP has ALD-coated pores with a direct-coupled anode that is designed to reduce per-pixel occupancies. The small pixel size makes conventional soldering impractical, so the prototype uses laser soldering. Efforts are ongoing to increase the fraction of pixels with reliable electrical connections. A first prototype has been characterised in the laboratory at Photek. A Lecroy WaveMaster 808zi-A scope has been used to read out four neighbouring pixels with a laser scanned across them. Fig. 1 shows the gain for each pixel as a function of laser position, which demonstrates the discrete pixel structure and shows that the point spread function is smaller than the fine-pixel dimension.

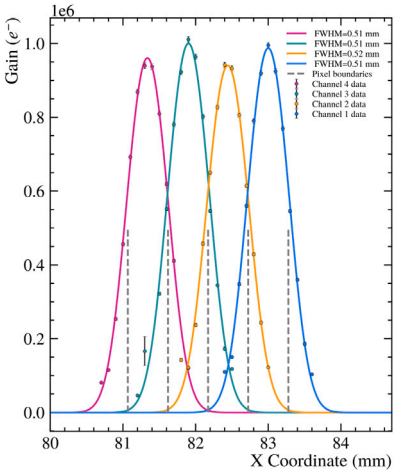

Fig. 1. Gain as a function of laser position from a scan over four pixels of the 16 × 96 MCP-PMT in the fine pixel direction. The vertical lines indicate the nominal pixel edges. The laser spot size is approximately 10 μm.

3. Assembly of a full-size module

The fused silica radiator plate, with a length 250 cm, is assembled from three separate quartz parts, each acquired from Nikon Glass.[1] The plates are bonded together using Epo-Tek 301-2 optical adhesive. The adhesive optical properties have been effective in the DIRC particle identification system for the BaBar experiment [5] and the Belle II TOP detector [6]. The same optical adhesive is used to bond the radiator plate to the focussing block. The bond line locations are shown in Fig. 2; the bottom two plates are 62.5 cm in length (two identical plates), and the uppermost plate is 125 cm long.

The supporting optical frame is designed to be as close as reasonably possible to a solution that could work in the context of the LHCb experiment. Hence a lightweight composite optical frame with low radiative length and low coefficient of thermal expansion has been chosen. This frame comprises a lower brace, two side braces and the focussing block mount (FBM). The quartz hangs from a thin aluminium ledge within the FBM, the so-called "letterbox". The optical frame is then mounted to an aluminium mounting frame that houses the MCP-PMTs and electronics. The electronics housing is attached on rails from which the module hangs, however, the structure has been designed so that it can also stand vertically, supported by rails at the bottom of the assembly if required.

Each of the constituent parts described above are mounted within an exoskeleton. The exoskeleton serves two purposes: it provides support and protection for the quartz when lifting and transporting, it also doubles as a bond jig to accurately position the quartz for bonding. The optical frame, electrical housing, and mounting rails are then assembled around the bonded quartz in situ. Light-tight panelling is mounted onto the exoskeleton for use in the test beam, and the TORCH prototype is retained in the exoskeleton for the duration of the test-beam campaign.

The focussing block is first roughly positioned, then fine adjustments are performed making use of a portable coordinate measuring machine (CMM). This is a vital starting point, as the quartz plates are positioned relative to the focussing block position. Fig. 3 shows a photograph of the focussing block positioned inside the FBM.

With the position of the focussing block finalised, the first quartz sheet is then positioned onto a sled. The sled's purpose is to provide a linear path of travel for the quartz sheets as they are being brought

[1] Nikon Corporation Glass Business Unit, Sagamihara-City, Kanagawa 252-0328, Japan.

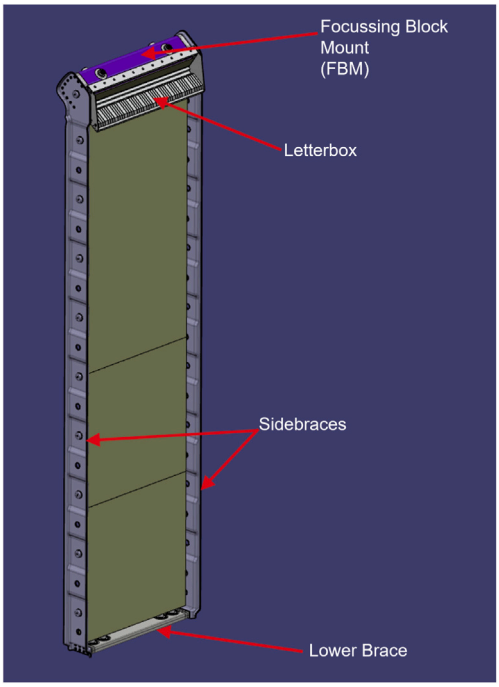

Fig. 2. Illustration of the main quartz optical frame components of the full sized TORCH demonstrator.

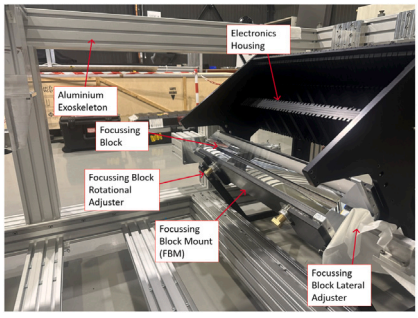

Fig. 3. Focussing block positioned inside the FBM.

to the bond position. Six micrometer-adjustable screws at the side and bottom position the quartz laterally while on the sled to align edges to the previous sheet, and to provide a very fine adjustment in the bond gap setting. The radiator plates are positioned roughly in a staging area at the base of the exoskeleton, shown in Fig. 4, then brought close to the bond location and positioned, then checked with the CMM until the correct position had been achieved. Plastic shims are then used to set the bond gap at 75 μm. Micrometer adjusters at the bottom of the sled are used to slowly push the sheet into contact, with the shims acting as spacers before they are removed.

Given the low viscosity of the Epo-Tek mixture, capillary action is used to draw the adhesive into the bond gap. The adhesive is applied in drops of 75 μL using a microlitre pipette. Drops were placed along the joint and the progression of the glue was visually monitored. Due to a small chamfer on the edges of the plates, a teflon-tape dam was used on the underside of the bond-line to catch any run-off of adhesive, to be later cleaned off with acetone and isopropyl alcohol. The bonding procedure is demonstrated in Fig. 5. Full cure is achieved in around 48 h, after which time the next plate is bonded in sequence.

Final steps involve installing the optical frame around the quartz inside the exoskeleton. The staging area for the sled is detached and replaced with the bottom bulkhead of the exoskeleton, ready for transport

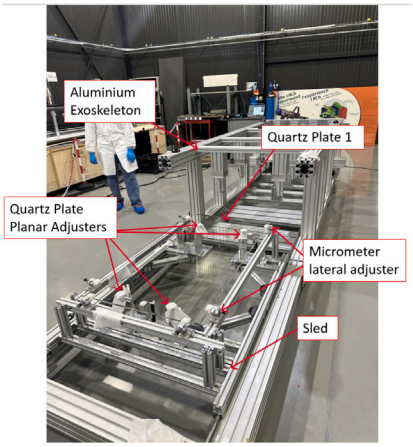

Fig. 4. Radiator plate on the sled in the staging area of the exoskeleton.

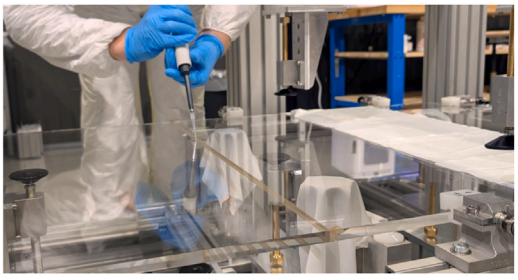

Fig. 5. The Epo-Tek application procedure, also showing the Teflon tape.

to the test beam area, and rotation into the upright position. Whilst the detector was assembled horizontally at Point 8 at CERN, it was operated vertically, and transport and rotation of the prototype was a critical step. The TORCH module inside the exoskeleton was transported in a truck over 16 km to the T9 experimental test-beam area of the CERN PS, rotated twice and craned in position multiple times, demonstrating the robustness of the structure.

4. 2025 beam test

4.1. Experimental setup

The module was tested at the T9 beamline in July 2025. The detector was exposed to beams of 5, 8 and 10 GeV/c momenta, comprising mainly pions and protons. The relative proportion of pions and protons depends on the beam momentum and is described in Ref. [7]. The different elements instrumenting the beam line are illustrated in Fig. 6.

A pair of CO_2-filled threshold Cherenkov counters is used to provide external PID information, followed by a large scintillator that can be used for trigger purposes. The beam passes first through an upstream timing station (T1) and then a downstream station (T2), located 10.4 m from T1, as illustrated in Fig. 6. The stations are identical and provide the two time references for each event. The timing stations are described in more detail in Section 4.2. An EUDET/AIDA silicon pixel telescope [8], comprising six Mimosa 26 planes and a FEI4 timing plane, is placed downstream and provides tracking information. This is particularly helpful to correctly describe the beam profile in simulations of charged particles entering the radiator. The TORCH module, hosted in the exo-skeleton described in Section 3 and instrumented with 6 MCP-PMTs, was placed on a pneumatic elevation table allowing to scan various beam-entry positions. Because of the weight of the prototype, it was not possible to scan horizontally. The performance of the TORCH

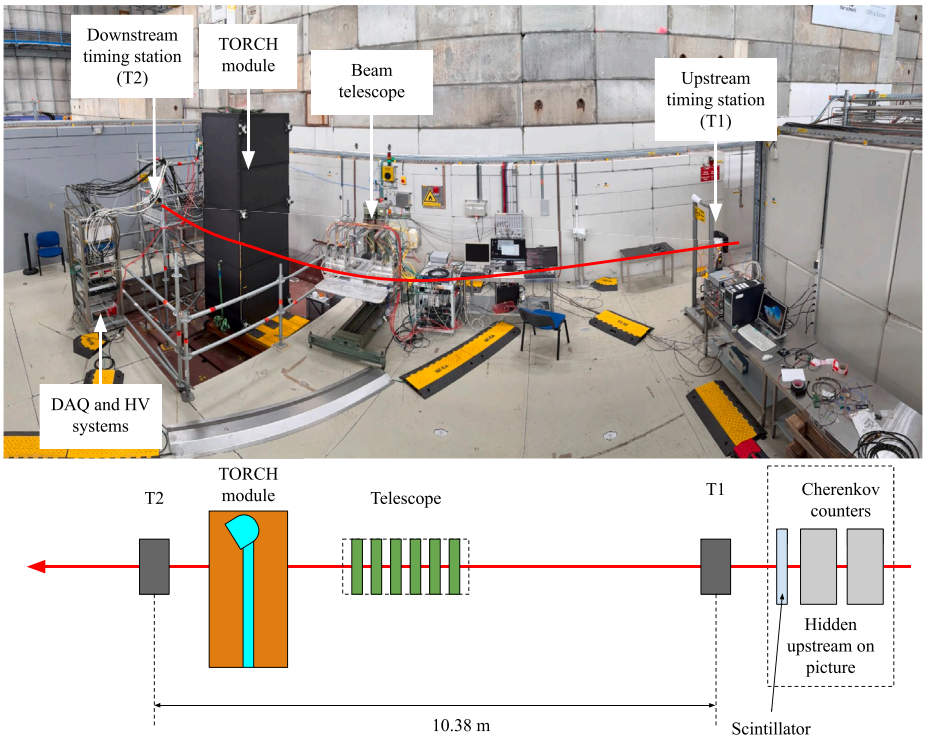

Fig. 6. Setup for the 2025 test beam in the T9 experimental area at CERN, with beam direction from right to left. The Cherenkov counters are not visible in the image to the right.

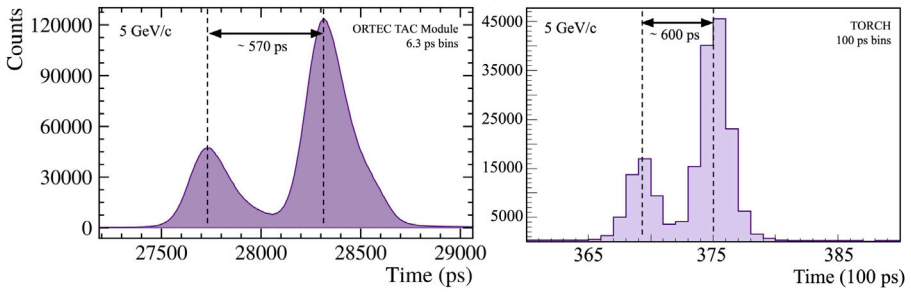

Fig. 7. Example time-of-flight spectra for a 5 GeV/c beam taken with the ORTEC TAC module (left) and TORCH module (right). The plots validate the expected beam composition by showing proton-pion separation.

module was studied for four beam-entry positions located 5 cm above and below each glue joint, primarily to evaluate the optical quality of the bonds.

4.2. Time reference system

Each timing station comprises a pair of crossed scintillators, used for triggering, as well as a $8 \times 8 \times 100\,\text{mm}^3$ borosilicate finger coupled to a single-channel MCP-PMT. When the crossed scintillators are positioned perpendicularly to the beam, the borosilicate finger is oriented so that the Cherenkov light produced by traversing particles is emitted directly towards the MCP-PMT to avoid delays due to internal reflections. This system is used to provide precise timing for each track and is used as a reference in the analysis. The timing signals obtained from the T1 and T2 timing stations are injected directly in the TORCH readout electronics to be digitised and saved as part of the event. These signals were also injected into an ORTEC Time-to-Amplitude Converter (TAC) module to verify that the expected time of flight distributions were obtained for each momentum.

4.3. Readout and trigger system

The trigger system consists of a combination of the two timing stations along with the Cherenkov counters and telescope shown in Fig. 6. For the timing station input to the global trigger, a coincidence signal between the two timing stations is used, where each timing-station signal comprises a coincidence between the discriminated scintillator signals and the borosilicate finger.

The readout of the TORCH detector consists of a custom readout chain consisting of NINO [9] and HPTDC [10] boards. The MCP-PMTs are connected to the NINO boards which amplify and discriminate the signals. This is fed into the HPTDC boards that provide fast measurements of both leading and trailing edges, allowing for time-walk corrections. Corrective measurements have also been made to account for non-linearities in the HPTDC time binning.

Fig. 7 compares the time of flight distributions obtained by the ORTEC module and the TORCH readout electronics after the data had been processed. In both cases, the expected separation is observed between pions and protons and the beam composition is observed to be consistent with that measured in [7].

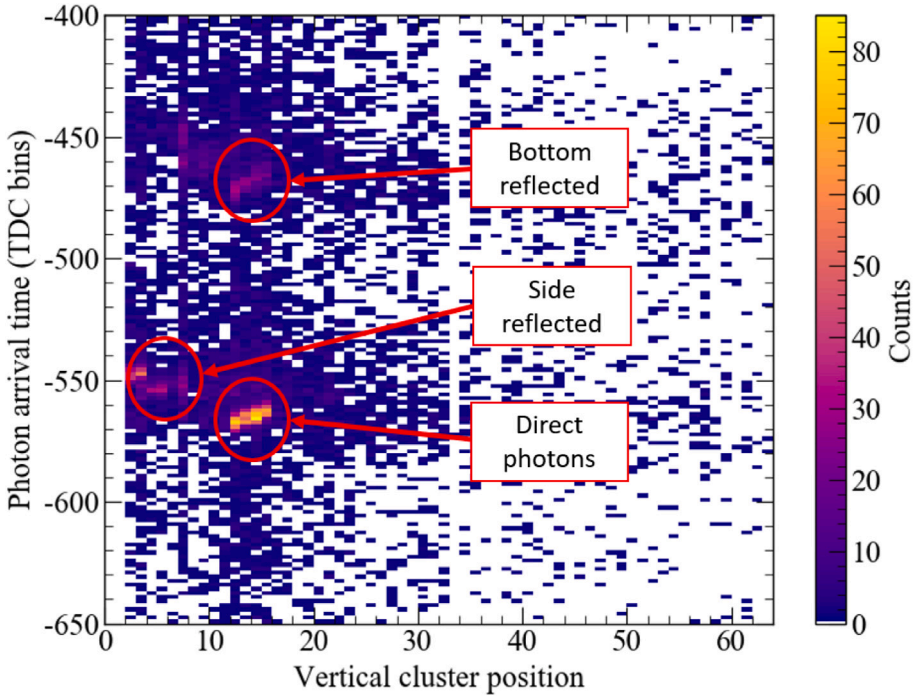

Fig. 8. Example distribution of photon arrival time (in TDC bins) versus vertical cluster position for photons arriving at a single horizontal pixel position. Direct and reflected photons are clearly separated.

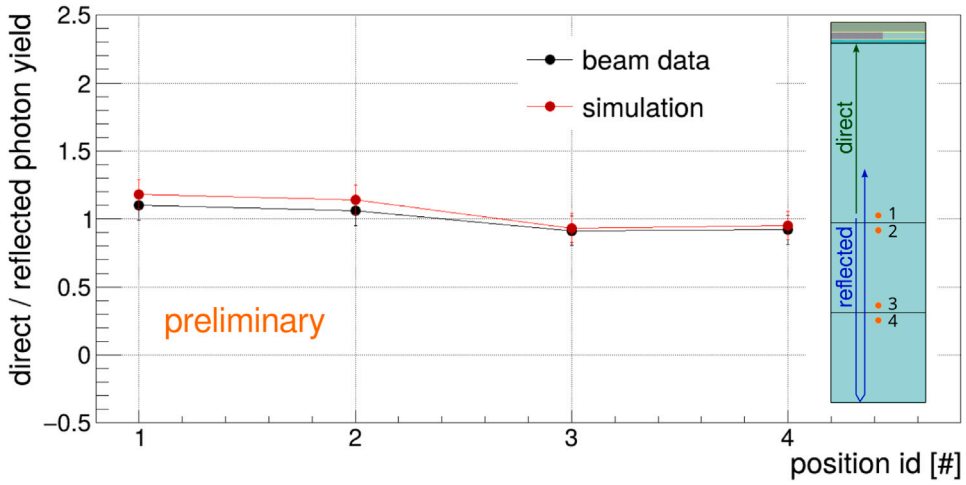

Fig. 9. Ratio of photon yields per event for two categories of photons. The first travel directly to the focusing block, while the second reflect from the bottom end of the plate, traversing a longer path and more glue joints. Results are shown for four beam positions at 5 GeV/c, as indicated in the inset. The red markers show the Geant 4 simulation.

4.4. Preliminary results: optical validation of bonded joints

A first objective of the beam test was to assess the optical quality of the bonded joints between the fused-silica radiator sections in the full-scale TORCH module. As described in Section 3, the radiator is manufactured in multiple pieces and assembled using optical adhesive, resulting in glue layers that Cherenkov photons must traverse before reaching the photodetector plane. Any significant photon loss or scattering at these interfaces would directly impact the detector performance and therefore must be carefully evaluated.

To probe the effect of the glue joints, data were taken at four vertical beam-entry positions, centred horizontally on the radiator plate. Positions 1 to 4 correspond to the beam impinging at normal incidence at locations: (1) 5 cm above the first (upper) glue joint of the radiator plates, (2) 5 cm below the same glue joint, (3) 5 cm above the second (lower) glue joint, and (4) 5 cm below the same glue joint. These positions were chosen such that, relative to the reference position located closest to the photon detectors (position 1), photons were required to traverse one or more additional glue layers before reaching the focusing block and MCP-PMTs. The reference position corresponds to the configuration with the minimum amount of intervening material

and therefore provides a baseline for comparison. For each beam-entry position, the average number of detected photons per event is measured after applying identical selection criteria. The photon yield per event is computed for each position and separately for direct photons (which travel directly to the photodetector plane) and reflected photons (which travel first to the bottom of the plate and then reflect back to the photodetector plane). Fig. 8 shows an example of the photon arrival time (in TDC bins) versus vertical pixel position of all photons arriving for a fixed horizontal position. The direct light and different reflection orders are clearly identifiable. Studying the ratio between direct and reflected photon yields allows a relative comparison that is largely insensitive to variations in beam conditions, trigger efficiency, and overall detector stability. The results of this preliminary analysis are shown in Fig. 9, which compares the beam test data with results from a stand-alone Geant 4 simulation. Within the statistical precision, no significant reduction in the relative photon yield is observed as the number of glue layers traversed by the photons increases. This indicates that no appreciable photon loss is introduced by the optical bonds and suggests that the bonding procedure preserves the required optical quality over the full module lengths. These results provide an important system-level validation of the radiator assembly strategy adopted for TORCH. More detailed studies, including position-dependent effects and comparisons with optical simulations, will be performed as part of future analyses using larger data samples.

5. Summary

The design, assembly and system-level validation of the first full-scale TORCH detector module have been presented. The module corresponds in size, geometry, and mechanical concept to a unit suitable for integration into the LHCb experiment and represents a significant step beyond previous small-scale prototypes. A mechanical assembly strategy based on a lightweight composite optical frame, rail-mounted support structure, and modular integration has been developed and successfully implemented.

Studies of Photek $53 \times 53\,\mathrm{mm}^2$- square customised MCP-PMTs with 8×64 and 16×96 granularities have been conducted in the laboratory. Further improvements in the gain retention at high rates and laser-solder connectivity for the 16×96 tube will be necessary to fulfil the TORCH requirements at the HL-LHC.

A beam test performed at the CERN PS in 2025 validated the operation of the TORCH detector chain, including timing reference systems, readout electronics, and photon detection. A preliminary analysis of the photon yield as a function of beam-entry position shows no significant loss associated with photons traversing multiple bonded interfaces, indicating that the optical quality of the glue joints meets requirements. Future analyses will focus on detailed timing performance and particle-identification capabilities.

Declaration of competing interest

The authors declare the following financial interests/personal relationships which may be considered as potential competing interests: Marion Lehuraux reports financial support was provided by UK Research and Innovation. Given their role as guest editors, R. Forty, N. Harnew and J. Schwiening had no involvement in the peer review of this article and had no access to information regarding its peer review. Full responsibility for the editorial process for this article was delegated to another journal editor. If there are other authors, they declare that they have no known competing financial interests or personal relationships that could have appeared to influence the work reported in this paper.

Acknowledgements

The authors would like to thank the PS staff and the CERN beam line operators for their support and for providing the high-quality particle beams used in this test beam campaign, specifically in the T9 area. The support of the Science and Technology Research Council, UK, is acknowledged.

References

[1] Framework TDR for the LHCb Upgrade II: Opportunities in Flavour Physics, and Beyond, in the HL-LHC Era, Technical Report, CERN, Geneva, 2021, URL: https://cds.cern.ch/record/2776420.

[2] M.J. Charles, R. Forty, LHCb Collaboration, TORCH: Time of Flight Identification with Cherenkov Radiation, Nucl. Instr. Meth. Phys. Res. Sect. A 639 (2011) 173–176, http://dx.doi.org/10.1016/j.nima.2010.09.021, arXiv:1009.3793.

[3] S. Bhasin, et al., Performance of a prototype TORCH time-of-flight detector, Nucl. Instr. Meth. Phys. Res. Sect. A 1050 (2023) 168181, http://dx.doi.org/10.1016/j.nima.2023.168181, arXiv:2209.13379.

[4] A. Markford, Rate capability and transient gain drop of a single photon timing detector, These Proc. (2026).

[5] I. Adam, et al., The DIRC particle identification system for the BaBar experiment, Nucl. Instr. Meth. Phys. Res. Sect. A 538 (1) (2005) 281–357, http://dx.doi.org/10.1016/j.nima.2004.08.129.

[6] J. Fast, et al., The Belle II imaging Time-of-Propagation (iTOP) detector, Nucl. Instr. Meth. Phys. Res. Sect. A 876 (2017) 145–148, http://dx.doi.org/10.1016/j.nima.2017.02.045, The 9th international workshop on Ring Imaging Cherenkov Detectors (RICH2016).

[7] E. Parozzi, et al., Secondary beam line efficiency studies at the CERN PS East Experimental Area, JACoW IPAC2024 (2024) TUPC52, http://dx.doi.org/10.18429/JACoW-IPAC2024-TUPC52.

[8] I. Rubinskiy, H. Perrey, An EUDET/AIDA Pixel Beam Telescope for Detector Development, PoS TIPP2014 (2014) 122, http://dx.doi.org/10.22323/1.213.0122.

[9] F. Anghinolfi, et al., NINO: An ultra-fast and low-power front-end amplifier/discriminator ASIC designed for the multigap resistive plate chamber, Nucl. Instr. Meth. Phys. Res. Sect. A 533 (2004) 183–187, http://dx.doi.org/10.1016/j.nima.2004.07.024.

[10] M. Mota, et al., A flexible multi-channel high-resolution time-to-digital converter ASIC, in: 2000 IEEE Nuclear Science Symposium. Conference Record (Cat. No.00CH37149), vol. 2, 2000, pp. 9/155–9/159, http://dx.doi.org/10.1109/NSSMIC.2000.949889.